Chemical Engineering Journal 497 (2024) 154515

Contents lists available at ScienceDirect

Chemical Engineering Journal

journal homepage: www.elsevier.com/locate/cej

Unleashing the power of precision drug delivery: Genetically engineered biomimetic nanodrugs incorporating liposomal polypharmacy against multidrug-resistant bacteria

Xianyuan Wei [a,b,c], Jintong Guo [b,c], Xiaorui Geng [b,c], Yuhao Chen [b,c], Xianfang Wei [d], Bin Liu [e], Jun Zheng [b], Zhen Yuan [b,c,*]

[a] Guangxi Key Laboratory of Special Biomedicine, School of Medicine, Guangxi University, Nanning 530004, China
[b] Faculty of Health Sciences, University of Macau, Macau SAR, China
[c] Centre for Cognitive and Brain Sciences, University of Macau, Macau SAR, China
[d] The MOE Key Laboratory of Biosystems Homeostasis & Protection and Innovation Center for Cell Signaling Network, Life Sciences Institute, Zhejiang University, Hangzhou 310058, China
[e] Emergency Department, Zhujiang Hospital, Southern Medical University, Guangzhou 510280, China

ARTICLE INFO

Keywords:
MDR
Multiple chemotherapeutics
Biomimetic liposome
Engineering outer membrane vesicles
Single chain fragment variable

ABSTRACT

To date, the antibiotics combination therapy is one of the most important approaches to eradicate the multidrug-resistant (MDR) bacteria. Besides, *in vivo* antibiotics delivery systems also play an essential role in improving the targeting and efficacy of antimicrobial therapies. Herein, we described a promising combination strategy by using an antibiotic medication (colistin) together with its adjuvant H-89 to treat MDR bacterial infections. Meanwhile, genetically engineered outer membrane vesicle (OMV) with single chain fragment variable (scFv) of anti-PcrV antibody (OMV-antiPAO1) was coated to liposomal colistin and H-89 to produce biomimetic nanodrugs (LNP-H89-Coli@OMV). In particular, the targeting, high-efficient delivery and enhanced killing abilities of LNP-H89-Coli@OMV to MDR bacteria is attributed to the OMV-antiPAO1, which show the similar structure and function to Gram-negative MDR bacteria and can express targeting antibody toward pcrV by the fusion of coding region with ClyA (a surface protein in *E. coli*). Antibacterial experiments demonstrated that LNP-H89-Coli@OMV was able to completely eliminate the persistent *Pseudomonas aeruginosa* PAO1 (>99.999999 % killing efficiency), whereas *in vivo* tests showed that MDR infections were totally cured by the present liposomal drugs for the first time. Therefore, this pilot study opened a new avenue for the development of multifunctional targeted drugs against MDR infection, particularly the persistent PAO1.

1. Introduction

The emergence of multidrug-resistant (MDR) bacteria is now becoming a serious threat to public health [1–3]. According to the reports from WHO, 80 % of present MDR is attributed to the overuse and misuse of antibiotics, rendering the once-effective antibiotics ineffective. In particular, with increased antibiotic resistance, the surviving bacteria under antibiotic pressure were able to spread the drug resistance widely at an alarming rate [4,5]. Herein, it is urgent to develop new antimicrobial protocols for the treatment of infection diseases while minimizing antibiotic dose and resistance at the individual level. Recently, there has been considerable interest in the application of combinational antibiotic regimens, which are designed to simultaneously engage multiple bacterial killing mechanisms, thereby delivering more efficacious approaches to combating multi-drug resistant pathogens [6–8]. Interestingly, colistin is widely recognized as the last-resort antibiotic against MDR Gram-negative pathogens. However, colistin also demonstrated its unignorable side effects such as nephrotoxicity and hepatotoxicity [9,10]. Meanwhile, N-[(2-p-bromo-cinnamylamino)ethyl]-5-isoquinolinesulfonamide (H-89) is able to serve as a protein kinase A (PKA) inhibitor, inhibiting structurally related kinases and inducing apoptosis of HeLa cancer cells [11–13]. Besides, it was discovered that H-89 compound can inhibit bacterial growth without compromising host cell viability [14–16]. In this study, a new combination strategy that combined colistin with its antimicrobial adjuvants H-89 was proposed to treat infections with lower antibiotic dose. To the

* Corresponding author at: Faculty of Health Sciences, University of Macau, Macau SAR, China.
E-mail address: zhenyuan@um.edu.mo (Z. Yuan).

https://doi.org/10.1016/j.cej.2024.154515
Received 1 February 2024; Received in revised form 23 June 2024; Accepted 1 August 2024
Available online 8 August 2024

best of our knowledge, this was the first study to inspect the underlying bactericidal mechanism of combined colistin and H-89. More specifically, the combination of traditional antibiotics with various antimicrobial compounds [17,18] can significantly reduce the individual side effects produced by drugs within the regimen, enhance the stability of bactericidal activity, and prevent the emergence of drug resistance [19,20].

In addition, biomimetic cell membrane-camouflaged nanocarriers is an emerging natural drug carrier, demonstrating its superior capability in improving biocompatibility and enhancing drug delivery efficiency and disease targeting with low immunogenicity [21–23]. Herein, the development of bacterial membrane vesicles-coated nanodrugs is also essential in antibacterial strategies to elevate its drug penetration into the bacteria, enhance accumulation of antibacterial drugs within the bacteria, and decrease collateral damage to normal microbiota [24–27].

However, the use of natural cell membrane exhibits its difficulty in precisely targeting the pathogen in infection regions [28]. By contrast, the antibody-antibiotic conjugate (AAC) can offer antibiotics with more precisely bactericidal capability *in vivo* [29]. In particular, the type III secretion system proteins pcrV with conserved sequence exposed on the surface of PAO1 are promising therapeutic antibody targets [30,31]. It has been demonstrated that pcrV monoclonal antibodies were as effective as the treatment with conventional antibiotics [32]. To date, due to the time-consuming and cost-intensive process of antibody purification, AAC has not been applied to large-scale antibacterial studies. Therefore, we proposed a novel targeted antibacterial strategy that was based on engineering outer membrane vesicle (OMV) with AAC. Different from traditional biomimetic cell membrane camouflage or AAC, genetically engineered OMV might exhibit considerable promise for improving drug delivery efficiency that can specifically target the bacteria and enlarge the therapeutic efficacy within a local region [25,33,34]. Previous studies have illustrated the targeted advantages of engineered OMV in cancer theranostics [35]. Likewise, genetically engineered OMV was constructed for the present work, serving as a targeted drug delivery system for killing MDR bacteria. Here, we engineered a *msbB* mutant *E. coli* (strain MG1655) that fused the ClyA coding region with scFv of bacterial antibody MEDI3902, ensuring that OMV was able to selectively target PAO1 for enhanced treatment of MDR infection (Fig. 1).

Meanwhile, to overcome the poor water solubility of H-89 and colistin, liposome were used as carriers for efficient encapsulation of the compounds (LNP-H89-Coli). The genetically engineered OMV-antiPAO1 was coated onto the surface of the LNP-H89-Coli to produce the novel nanaodrugs (LNP-H89-Coli@OMV). The proof-of-concept tests of LNP-H89-Coli@OMV were carried out by using both *in vitro* and *in vivo* experiments. Our findings illustrated that LNP-H89-Coli@OMV can deliver antibiotics to the targeted infected sites with high efficacy, demonstrating its superior bactericidal ability for the treatment of biofilm infection and eradication of MDR bacteria like *Pseudomonas aeruginosa* with a much lower dosage.

More importantly, the antibacterial mechanism of LNP-H89-Coli@OMV was also inspected for the present work. We revealed that colistin was able to disrupt the bacterial membrane and facilitated the efficient entry of H-89 into cytoplasm. In addition, it was revealed that H-89 can induce apoptosis-like bacteria death, by comprehensively exploring the apoptosis hallmarks, including DNA fragmentation, chromosome condensation, caspase activation, membrane depolarization, phosphatidylserine exposure, and cell filamentation. Further proteomics analysis showed that H-89 might target MiaA protein for improved bactericidal ability of LNP-H89-Coli@OMV. Meanwhile, the genetically engineered component of LNP-H89-Coli@OMV can enhance the treatment efficacy of biofilm infection and its targeting capability in infected regions. In summary, a combination strategy that utilized genetically engineered biomimetic nanodrugs was inspected for high-efficacy elimination of MDR bacteria. Therefore, this pilot work might open a new avenue for the development of novel targeted liposomal drugs to kill MDR bacteria.

1.1. Design, preparation, and characterizations of LNP-H89-Coli@OMV

To synthesize LNP-H89-Coli@OMV, LNP-H89, LNP-H89 and LNP-Coli, H-89 or (and) colistin were encapsulated in the sterically stabilized liposomes (Figs. 1a and 2). Here, liposomes (LNP) were produced with 1,2-dipalmitoyl-*sn*-glycero-3-phosphocholine (DPPC), 1,2-Dimyristoyl-*sn*-glycero-3-phosphoglycerol (DMPG) and cholesterol, after repeatedly extruded through 100-nm membrane by Avanti Mini-extruder. Transmission electron microscopy (TEM) images demonstrated that LNP-Coli (Fig. 2a), LNP-H89 (Fig. 2b), LNP-H89-Coli (Fig. 2c) and LNP-H89-Coli@OMV (Fig. 2d) were uniformly distributed and spherical in shape with an average size of approximate 146 nm. In particular, LNP-H89-Coli@OMV were produced with bioengineered OMV, exhibiting a typical OMV structure of gram-negative bacteria (Fig. 2d).

To produce OMV, we engineered *Escherichia coli* (*E. coli*) to express the desired protein and then coated the extracted OMV onto LNP-H89-Coli to produce LNP-H89-Coli@OMV. In addition, gene editing technology was utilized to construct the plasmid pBAD_*clyA*-antiPAO1-flag (Fig. S1) and an in-frame deletion mutant of *ΔmsbB* in *E. coli* MG1655. The fused protein ClyA- antiPAO1-flag contains three components including variable domain of MEDI3902 antibody scFv [36] of heavy chain and kappa chain (antiPAO1), flag tag in C-terminal (antiPAO1-

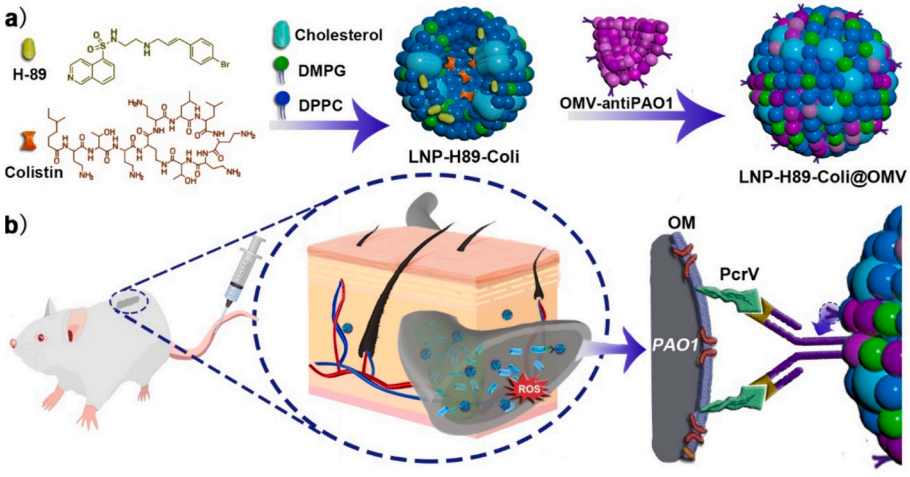

Fig. 1. The prepared LNP-H89-Coli@OMV with antibacterial activity. (a) Synthesis process of LNP-H89-Coli@OMV. (b) Schematic of LNP-H89-Coli@OMV for targeting MDR *PAO1* and treatment of skin biofilm infection by MDR bacteria.

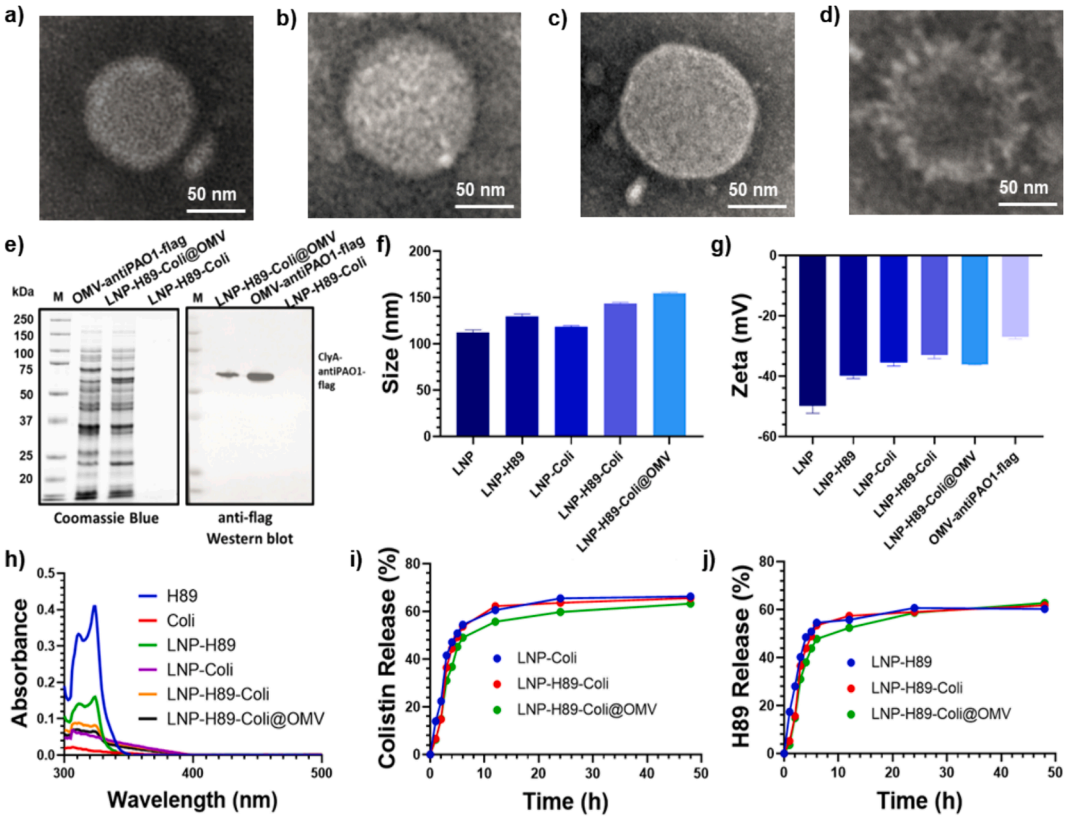

Fig. 2. Characterization of LNP-H89-Coli@OMV. TEM images of LNP-Coli (a), LNP-H89 (b), LNP-H89-Coli (c), and LNP-H89-Coli@OMV (d). (e) The detection of ClyA-antiPAO1-flag fusion protein by western blot and SDS page analysis on OMVs and LNP-H89-Coli@OMV, respectively, by using an anti-flag antibody. (f) Size distributions of LNP, LNP-H89, LNP-Coli, LNP-H89-Coliand LNP-H89-Coli@OMV measured by Dynamic light scattering (DLS). (g) Zeta potentials of LNP, LNP-H89, LNP-Coli, LNP-H89-Coli, LNP-H89-Coli@OMV, and OMV-antiPAO1-flag. (h) UV–vis absorption spectra of H89, Coli, LNP-H89, LNP-Coli, LNP-H89-Coli, and LNP-H89-Coli@OMV. (i) Colistin release profiles under LB medium at room temperature with 220 rpm. (j) H-89 release profiles under LB medium at room temperature with 220 rpm. Here, LNP denotes liposome, LNP-Coli denotes liposomal colistin, LNP-H89 denotes liposomal H89, and LNP-H89-Coli denotes liposomal colistin and H89.

flag), and the bacterial outer membrane protein ClyA (ClyA-antiPAO1-flag). Interestingly, the bispecific antibody MEDI3902 of VH and V-kappa contained complementarity determining region CDR1, CDR2 and CDR3, which was able to target PcrV component of the type III secretion system [31]. Meanwhile, the knockout of *msbB* gene for the present study was derived from an under-age type of pentaacylated lipopolysaccharide OMV, demonstrating reduced endotoxicity and side effects [37,38].

The successful expression of ClyA-antiPAO1-flag fused protein in *ΔmsbB* (pBAD_*clyA*- antiPAO1-flag) strain under L-arabinose inducing, was inspected by using SDS page (Fig. S2) and Western blot (Fig. S3) with a predicted protein weight of 63.1 kDa. Therefore, we first extracted endotoxic OMV-antiPAO1 and identified the ClyA- antiPAO1-flag on their surface (Figs. S4–S6). The mixture of fresh OMV and prepared LNP-H89-Coli were repeatedly extruded through 100-nm membrane by Avanti Miniextruder, whereas the mechanical force facilitated membrane fusion of OMV with LNP-H89-Coli. The successful fusion was demonstrated by SDS page and Western blot (Fig. 2e). In addition, gradually increased nanoparticle sizes measured by DLS (Fig. 2f) and decreased zeta potentials (Fig. 2g) further confirmed the fusion process of LNP-H89-Coli and OMV. It was revealed that the constructed LNP-H89-Coli@OMV had a diameter of around 156 nm while the zeta potential decreased to the level of OMV. Further, the optical absorption spectra of colistin and H-89 was measured. The absorption peaks around 330 nm also illustrated the successful loading of colistin and H-89 in liposome (Fig. 2h). Besides, the loading or encapsulated rate of H-89 and/or colistin inside LNP-H89, LNP-Coli and LNP-H89-Coli was respectively examined and listed in Fig. S7 and Table S1. Meanwhile, to inspect the efficacy of drug release, a number of experiments were carried out at 37℃ with 200 rpm. It was revealed that the release rate of H-89 and colistin in LNP-H89-Coli@OMV can be up to 60 % at 12 h, respectively. (Fig. 2i and j). More specifically, we demonstrated that at 4 °C storage, the H-89 and colistin leakage in LNP-H89-Coli@OMV was less than 5 % after one-week storage while that was less than 8 % after an extended storage period of 40 days (Figs. S8 and S9). DLS and zeta potentials results further demonstrated that LNP-H89-Coli@OMV were with excellent stability in water or physiological medium (Figs. S10 and S11), exhibiting their potential for *in vivo* applications.

1.2. In vitro bactericidal ability of LNP-H89-Coli@OMV against MDR bacteria

In this section, *in vitro* tests were carried out for LNP-H89-Coli@OMV to inspect its antimicrobial ability against antibiotic-resistant bacteria. The structure of LNP-H89-Coli@OMV mainly consists of two components, namely H-89 and colistin. To examine the synergism between H-89 and various antibiotics like colistin (Fig. 3a), kanamycin (Fig. 3b), ampicillin (Fig. 3c) and norfloxacin (Fig. 3d), the checkboard analysis was performed using model *E. coli* MG1655. As displayed in Fig. 3e, H-89 exhibited the best synergism with colistin against gram-negative bacteria according to calculated fractional inhibitory concentration index (FICI) value [39]. Our subsequent experiments demonstrated that the reason for this synergistic effect is because colistin disrupted bacterial membrane structure and resulted in the accumulation of H-89 (Fig. S12). The checkboard analysis was further performed with MDR bacteria *Escherichia coli(p_mcr-1), Citrobacter rodentium, Salmonella*

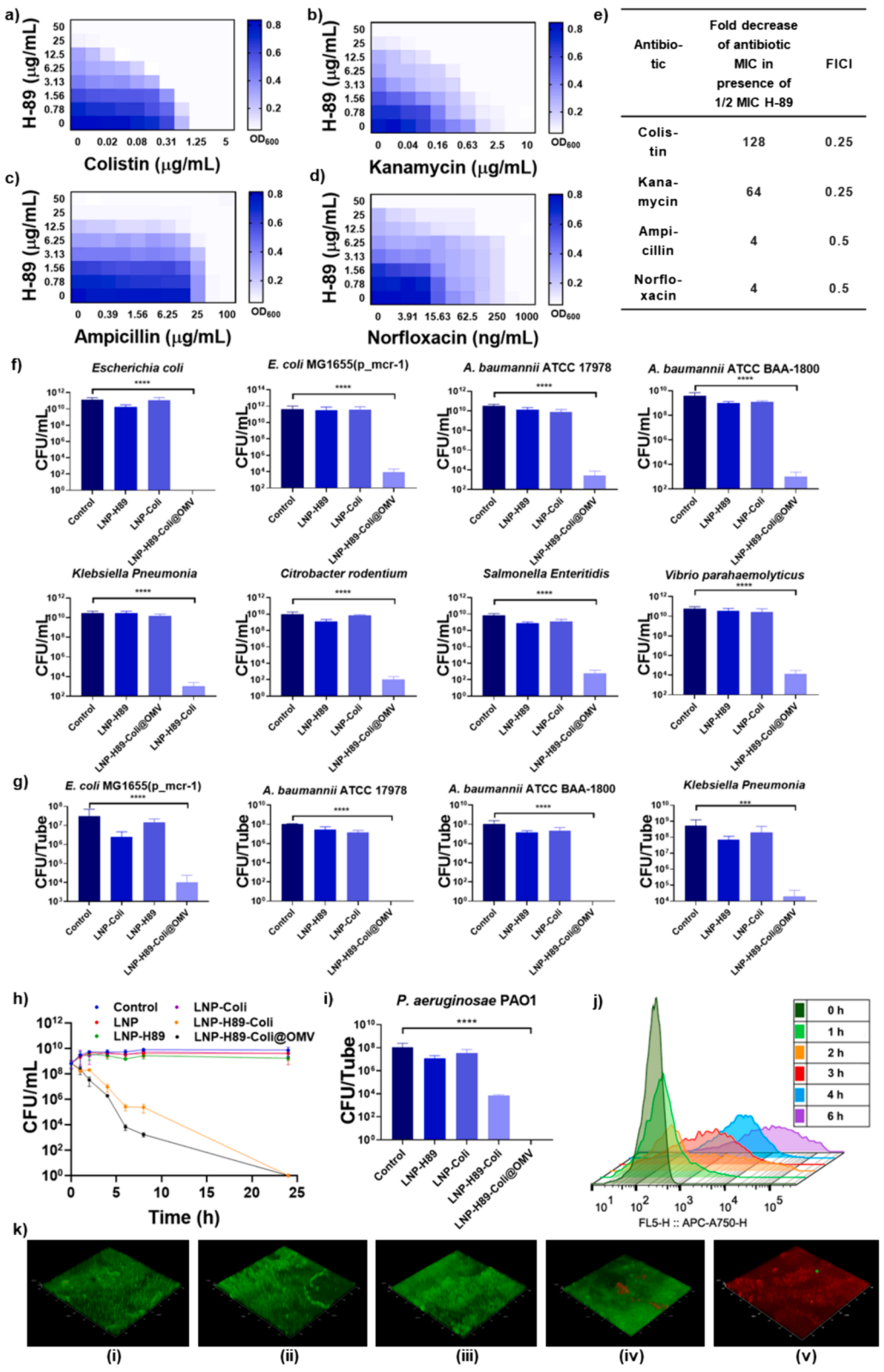

Antibiotic	Fold decrease of antibiotic MIC in presence of 1/2 MIC H-89	FICI
Colistin	128	0.25
Kanamycin	64	0.25
Ampicillin	4	0.5
Norfloxacin	4	0.5

Fig. 3. Bacterial killing ability of LNP-H89-Coli@OMV against MDR bacteria. Checkerboard plots for the antibacterial activity of H-89 in combination with colistin (a), kanamycin (b), ampicillin (c), and norfloxacin (d) with various amounts of doses. (e) FICI values for H-89 in combination with various antibiotics. (f) Survival of exponential-phase MDR bacteria associated with different treatments. (g) Survival of persistent MDR bacteria in biofilm with different treatments. (h) Growth curve of bacterial killing under different treatments in *PAO1*. (i) Survival of biofilm *PAO1* with different treatments. (j) Bacterial uptake of LNP-H89-Coli@OMV@DiR by flow cytometry at various time points. (k) Detection of live/dead biofilm in persistent PAO1 for different treatment groups: (i) Control, (ii) LNP-H89, (iii) LNP-Coli, (iv) LNP-H89-Coli, and (v) LNP-H89-Coli@OMV. The live and dead bacterial stained with Syto9 (green) and PI (red), respectively. Here, LNP-Coli denotes liposomal colistin, LNP-H89 denotes liposomal H89, and LNP-H89-Coli denotes liposomal colistin and H89. (For interpretation of the references to colour in this figure legend, the reader is referred to the web version of this article.)

Enteritidis ATCC13076, Acinetobacter baumannii ATCC 17978, Klebsiella pneumoniae ATCC BAA-2146 and *Vibrio parahaemolyticus*, strongly indicating that H-89 can serve as the best adjuvant of colistin (Fig. S13). Due to the synergistic effect in MDR bacteria killing, colistin and H-89 can respectively work as antibacterial agents and adjuvants of the antibiotics combination therapy for enhancing bactericidal activity. Then we loaded colistin and H-89 into liposomes to enhancing water solubility, reducing toxicity, and improving drug delivery capabilities.

In order to validate the antibacterial performance of the nanomaterials synthesized with success, we undertook a series of Minimum Inhibitory Concentration (MIC) assays. Our findings indicated that the LNP-H89-Coli@OMV nanomaterial exhibited a remarkably low MIC value of 226.5 μg/mL, as detailed in Table S2, thus confirming its significant potential as an effective antimicrobial agent. In addition, planktonic cultures of *Escherichia coli, Escherichia coli(p_mcr-1), Acinetobacter baumannii* ATCC 17978*, Acinetobacter baumannii* ATCC BAA-1800*, Klebsiella pneumoniae* ATCC BAA-2146*, Citrobacter rodentium DBS100, Salmonella Enteritidis* ATCC13076 and *Vibrio parahaemolyticus,* were treated with LNP-H89-Coli@OMV in their late exponential growth phase. The killing assay demonstrated that LNP-H89-Coli@OMV induced the most effective killing for MDR pathogens (Fig. 3f). Meanwhile, LNP-H89-Coli@OMV exhibited significant killing capability in persistence bacteria by biofilm cultures of *Escherichia coli(p_mcr-1), Acinetobacter baumannii ATCC 17978, Acinetobacter baumannii ATCC BAA-1800* and *Klebsiella pneumoniae ATCC BAA-2146* (Fig. 3g). We also demonstrated that the killing performance of LNP-H89-Coli@OMV is quick and time-dependent in the late exponential growth phase of PAO1 (Fig. 3h). LNP-H89-Coli@OMV exhibited approximately 100-fold antibacterial efficacy as compared to LNP-H89-Coli after 8 h of treatments (Fig. 3h). In persistence bacteria, OMV showed quick sterilization (Fig. 3i). Flow cytometry analysis confirmed that LNP-H89-Coli@OMV was rapidly internalized to bacteria (Fig. 3j; Figs. S14 and S15). Similar confocal microscopy imaging findings were identified according to the uptake of persistent PAO1 pathogens (Fig. S16). We further explored the survival of persistent pathogens (Fig. 3k), and demonstrated that almost all bacteria treated with LNP-H89-Coli@OMV were dead (red fluorescence), indicating that LNP-H89-Coli@OMV has remarkably eliminating effect on biofilm survival. Taken together, our findings revealed the superior antibacterial properties of LNP-H89-Coli@OMV against planktonic and persistent pathogens *in vitro*.

1.3. The underlying antibacterial mechanism of LNP-H89-Coli@OMV

In this section, the antibacterial mechanism of LNP-H89-Coli@OMV against MDR infections were carefully inspected. Firstly, the mechanism of colistin, as the last line of defense against MDR bacteria, has been systematically and thoroughly studied. Basically, colistin can interact with lipopolysaccharides and *phospholipid A* upon the bacterial cell membrane, destroying the potential and integrity of cell membrane and interfering the normal function of bacterial membrane [9,40]. The leakage of cell contents and intake of exogenous substances, reduce the resistance of bacteria to other antibiotics and enhance the bactericidal effect of other antibiotics under non-lethal concentration of colistin [41,42]. For the combination therapy that integrates colistin and H-89, colistin with sub-lethal concentration might mediate the destruction of bacterial membrane, further promoting the accumulation of H-89 and enhancing the bactericidal ability (Fig. S12).

By contrast, H-89 as the new antibacterial compound was rarely used for antibacterial tests and its underlying bactericidal mechanism is yet unclear. Previous reports demonstrated that H-89 compound was able to induce apoptosis in eukaryote cell [12,13]. Therefore, we examined its killing behavior (Fig. S17) and then detected the apoptosis-like death (ALD) hallmarks under H-89 treatments at proper killing time points (Fig. 4a). Interestingly, a remarkable positive level of green DCF fluorescence were captured by confocal microscopy imaging (Fig. S18) and flow cytometry (Fig. 4a; Fig. S19), strongly indicating that H-89 induced ROS generation. Besides, to examine the characteristic biomarkers of apoptosis including caspase increase, membrane depolarization and phosphatidylserine exposure, the FITC-conjugated peptide pan-caspase inhibitor Z-VD-FM, fluorescently labeled $DIBAC_4$ and fluorescently labeled annexin V dyes were used, respectively. Significantly high fluorescence intensity detected by flow cytometry clearly revealed the existence of caspase increase, membrane depolarization and phosphatidylserine exposure during the initial phase of apoptosis induced by H-89 (Fig. 4a; Figs. S20–S22).

Further, terminal deoxynucleotidyl transferase dUTP nick-end labeling (TUNEL) assay was performed to investigate DNA fragmentation. We demonstrated that only FITC-conjugated dUTP signals were detected in LNP-CHE-Coli treatments, suggesting that the killing process was accompanied with DNA fragmentation (Fig. 4a; Fig. S23). Besides, the structure of bacterial chromosome was monitored by confocal microscopy imaging with nuclear-specific dye, Hoechst 33,342 and PI stains. Interestingly, the Hoechst and PI exhibited increased fluorescence signals in the presence of H89, indicating that the killing process was indeed accompanied with chromosome condensation (Fig. 4b).

More importantly, previous studies illustrated that RecA is an important caspase-like protein in ALD [43]. The ALD hallmarks were significantly decreased due to the antibiotic norfloxacin in *recA* mutant. Meanwhile, ClpX and ClpP were also recognized as two important ALD-related proteins[35]. To examine whether caspase-dependent ALD induced by H-89 was also relevant to RecA, the *E. coli* of △*recA*, △*clpX* and △*clpP* were produced by suicide plasmid and homologous arm exchange and then the outcomes of knockout gene were successfully verified by PCR. We demonstrated that western blot revealed significant reduction in the expression of RecA protein (Fig. 4c). We detected H-89 MIC in △*recA*, △*clpX* and △*clpP* strains, but demonstrated that no significant difference was detected between them and those from the wild type (Table S3). Therefore, H89-induced ALD was not related to recA, clpX, and clpP. As illustrated in Fig. 4d, the remarkable positive signals of ALD were detected by flow cytometry as compared to that of the control group under△*recA*, which included the ROS level (Fig. S24), caspase increase (Fig. S25), membrane depolarization (Fig. S26), phosphatidylserine exposure (Fig. S27), DNA fragmentation (Fig. S28), and chromosome condensation (Fig. S29). Taken together, these findings deepen our understanding of the H-89 antibacterial mechanism, illustrating that the antibacterial effect was due to the induced ALD rather than relevant to RecA, ClpX or ClpP protein.

To further inspect the bactericidal mechanism of H89, we performed proteomic and bioinformatics analysis under H-89 treatment of MG1655. In particular, quantifiable proteins were identified in the three biological replicates. Fig. 4e demonstrated the results from proteomics coupled with bioinformatics analysis in H-89 treatment. The data were analyzed by GO enrichment analysis in Biological Process, Cell Component as well as Molecular Function. The differential expressions of proteins were demonstrated in volcano (Fig. 4f) and column diagram (Fig. 4g). The red dots represented the proteins up-regulated while the green dots denoted proteins down-regulated. The gray dots denoted the proteins with no change in abundance between the two groups. Proteins with an adjusted P value <0.05 and abundance fold change >2 or <0.5 were assigned as differential expression between the two groups. We subsequently analyzed the genes that had significant changes in the proteome analysis. The screening experiments were performed under 2-fold MIC concentration of H-89 in KEIO library. As displayed in Fig. 4h, the screening results revealed several potentially H89-related genes. Besides, we analyzed the killing assay in the three strains *miaA*::Kan, *pyrE*::Kan and *cpxP*::Kan, illustrating that the bactericidal ability of H-89 was significantly reversed in *miaA*::Kan (Fig. S30). Since the *E. coli* strain in the KEIO library is BW25113, we also performed MIC testing in the experimental strain MG1655 by constructing in-fusion *miaA* mutant. We demonstrated that the MIC of H-89 in *miaA* mutant increased significantly as compared to that of wild type MG1655 (Table S4). Study indicates that the selection pressure exerted by ciprofloxacin on *miaA* gene

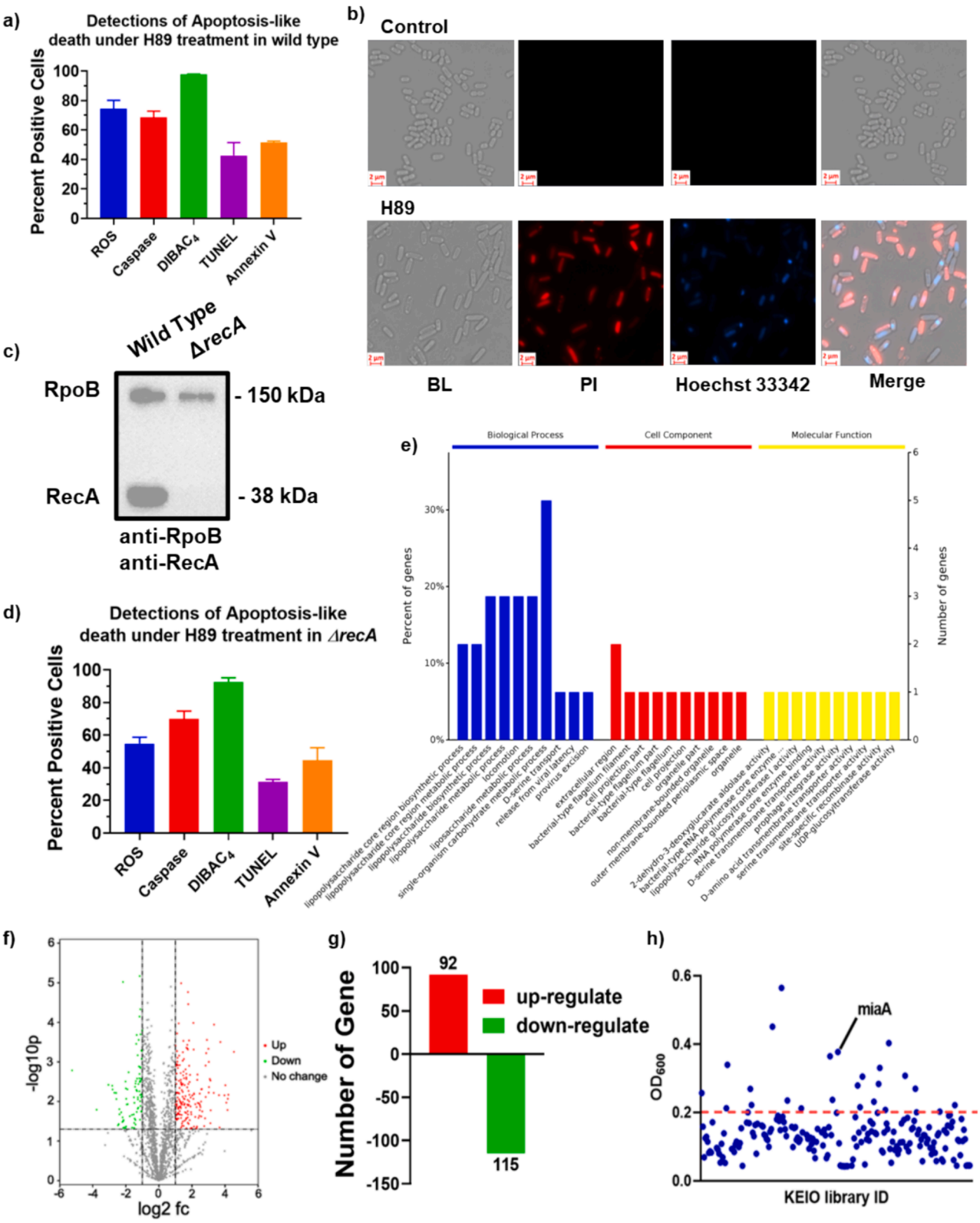

Fig. 4. *In vitro* antibacterial efficacy of H-89. (a) The percent change in ROS, caspase, membrane depolarization, DNA fragmentation and PS exposure exhibited by MG1655 strain under H-89 treatment. (b) Detection of chromosomal condensation by fluorescence imaging of MG1655 under H-89 treatment. (c) The detection of RpoB and RecA protein expression by western blot. (d) The percent change in ROS, caspase, membrane depolarization, DNA fragmentation and PS exposure exhibited by Δ*recA* strain under H-89 treatment. (e) GO classification of differentially expressed proteins under H-89 treatment. (f) Volcano plot showing proteins with differential expression under H-89 treatment. (g) Up-regulated and down-regulated genes under H-89 treatment. (h) Detection of potential target gene from *E. coli* knock out library under H-89 treatment.

knockout strains leads to multidrug resistance against chloramphenicol, streptomycin, and ciprofloxacin itself, which underscores the pivotal role of *miaA* deletion mutations in enhancing antibiotic resistance [44]. This observation aligns with our experimental results, where the deletion of the *miaA* gene was found to confer resistance to the antibiotic H89. As a critical enzyme for tRNA isopentenylation, MiaA mediates modifications essential for accurate recognition of codons by tRNAs and for maintaining fidelity during the translation process. Mutations in MiaA can potentially result in the inability of certain tRNAs to undergo effective modification, thereby impacting mRNA translation efficiency and accuracy, ultimately contributing to an increase in bacterial mutation rates [45]. Consequently, the bactericidal effect of H-89 is not influenced by overexpression of the miaa protein (Fig. S31). Under H-89 treatment conditions, the upregulated expression of MiaA suggests that bacterial cells may attempt to compensate for potential tRNA under-modification caused by H-89 interference by increasing the levels of

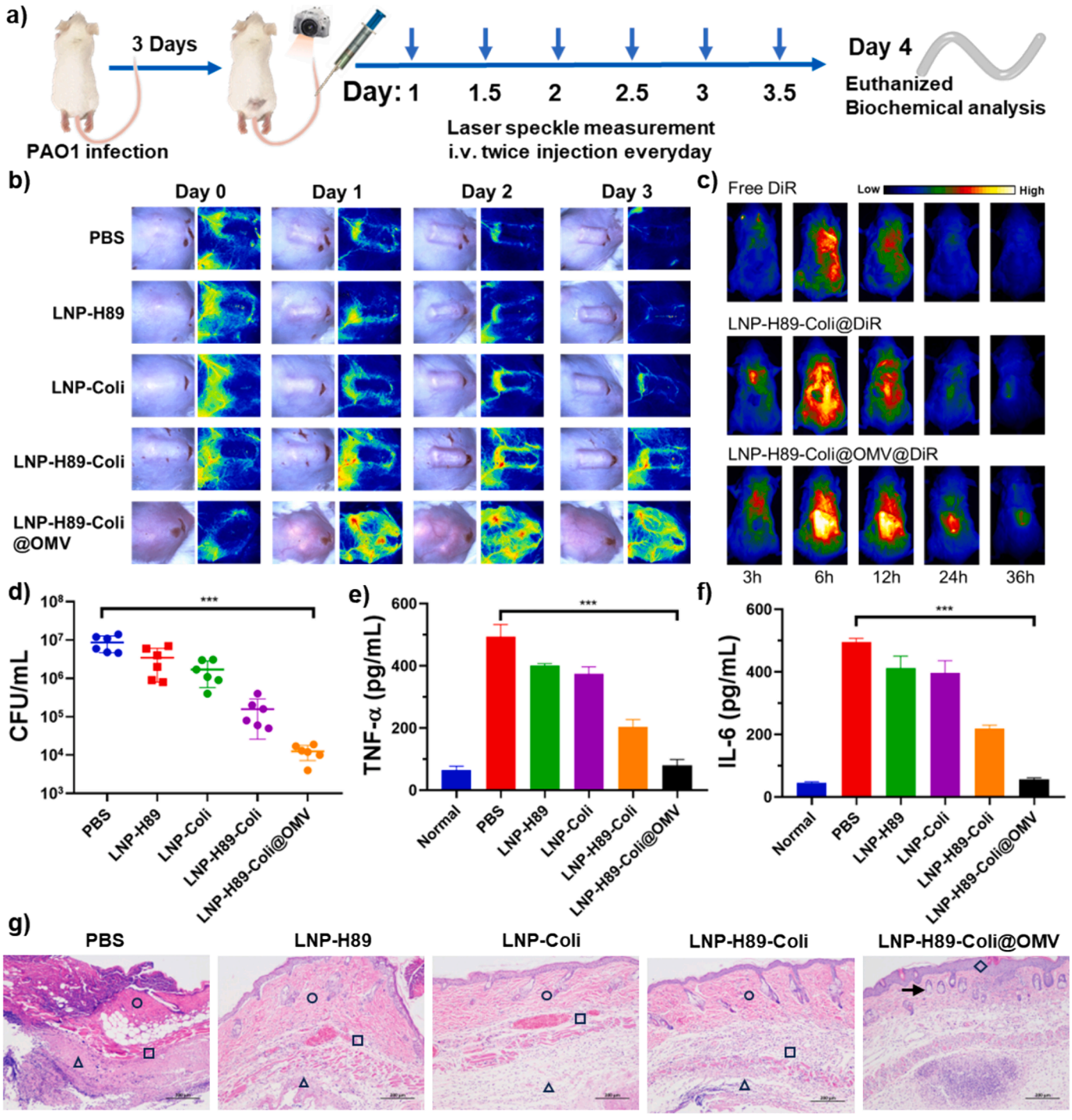

Fig. 5. Antibacterial effects of LNP-H89-Coli@OMV *in vivo*. (a) Schematic of the construction and treatment process of biofilm infection. (b) *In vivo* laser speckle imaging of the blood flow of the biofilm mice with different treatment groups. (c) Biodistribution analysis by fluorescence imaging of biofilm mice at different time points. (d) Bacterial counting analysis of biofilm *in vivo* for different treatment groups. (e) ELISA analyses of TNF-a in serum of biofilm infected mice after different treatments. (f) ELISA analyses of IL-6 in serum of biofilm infected mice after different treatments. (g) Skin tissue histology after H&E staining in biofilm infected mice under different treatments.

tRNA modifying enzymes (Fig. S32). Moreover, H-89 significantly downregulates the expression of TrpR (tryptophan synthase repressor) and TnaA (tryptophan transaminase) [46], while significantly upregulating PheS (phenylalanine-tRNA ligase alpha subunit), indicative of induced deficiencies in intracellular tryptophan and phenylalanine within the bacteria (Fig. S32). Taken together, our findings demonstrated that the killing mechanism of H-89 was strongly relevant to *miaA*.

1.4. Biosafety and targeting ability of as-prepared LNP-H89-Coli@OMV

The efficacy of LNP-H89-Coli@OMV for the treatment of MDR infections was also examined *in vivo* (Fig. 5a) and the presently *in vivo* test protocol was approved by the Ethics Committees of the University of Macau.

We first tested the biosafety of LNP-H89-Coli@OMV according to the cell viability experiments, histological and blood biochemical analysis. It was revealed that LNP-H89-Coli@OMV exhibit no effect on the viability of normal cells with the incubation for 24 h and concentrations up to 50 μg/mL (Fig. S33). In addition, histological analysis of the major organs, such as the heart, liver, spleen, lung, and kidney was carried out, suggesting that LNP-H89-Coli@OMV caused no overt tissue damage after the treatment of MDR infections (Fig. S34). In particular, blood biochemical analysis was also performed, showing minimal changes 14 days post-intravenous injection as compared to that of the control group (Fig. S35).

Further, the *in vivo* targeting ability of LNP-H89-Coli@OMV was inspected and compared to that of uncoated nanodrugs. We demonstrated that LNP-H89-Coli@OMV exhibited significantly longer accumulation time to biofilm PAO1 with higher concentrations in intravenous catheter as compared to uncoated OMV group (Fig. 5c; Fig. S36).

1.5. In vivo tests of LNP-H89-Coli@OMV for the treatment of MDR infections

To access the therapeutic effect of LNP-H89-Coli@OMV *in vivo*, we developed persistent PAO1 infection model by intravenous biofilm-catheter placement in BALB/c. In this study, the mice were randomly assigned to five treatment groups after performed biofilm placement surgery: (1) Control (2 mg/kg), (2) LNP-H89 (2 mg/kg, contain H-89 ~ 20 μg/kg), (3) LNP-Coli (2 mg/kg, contain coli ~ 2 μg/kg), (4) LNP-H89-Coli (2 mg/kg, contain H-89 ~ 20 μg/kg and coli ~ 2 μg/kg), and (5) LNP-H89-Coli@OMV (2 mg/kg, contain H-89 ~ 13.33 μg/kg and coli ~ 1.33 μg/kg). Treatments were conducted one day after bacterial infection surgery. Laser speckle imaging was used to monitor the changes of subcutaneous blood vessels during the progression of infection (Fig. 5b). We demonstrated that subcutaneous blood flow in mice back significantly decreased 1 day post-bacterial infection. However, for the groups treated with LNP-H89-Coli@OMV, we demonstrated that more blood vessels were gradually regenerated, subcutaneous blood flow gradually increased, and the whole lesion volume was significantly reduced (Fig. 5b). The changes of structural and functional information in the lesion region indicated that the treatment was highly effective in promoting the recovery from the MDR infectious. Our findings also demonstrated that the treatment dramatically reduced the bacterial load, resulting in approximately 1000-fold fewer bacteria in the infection region as compared to that of non-treatment groups (Fig. 5d). Enzyme-linked immunosorbent assay (ELISA) of immune factors was performed to reveal the inflammatory response *in vivo* and assess the severity of inflammation caused by bacteria. As illustrated in Fig. 5e and f, the pro-inflammatory cytokines TNF-α and Interleukin-6 (IL-6) in LNP-H89-Coli@OMV treatment group significantly decreased as compared to those from the control groups, indicating that the severity of inflammation caused by persistent PAO1 infection in the skin was significantly reduced due to the use of LNP-H89-Coli@OMV. We then performed H&E staining on the lesioned skin tissue infected by persistent PAO1. Histological analysis demonstrated significantly necrotic area (circle marked area), capillary congestion (square marked area), and mixed inflammatory infiltrate composed of mononuclear/polynuclear cells (triangle marked area) for the first four treatment groups (Fig. 5g). By contrast, significantly decreased necrotic area with inflammatory infiltrate, obviously increased subcutaneous adipocytes (arrow marked area) and intact epidermis (rhombic marked area), further confirmed that LNP-H89-Coli@OMV exhibited high efficacy in the treatment of persistent PAO1 infection. It is very hard to eradicate PAO1 biofilm inside intravenous catheter *in vivo* due to the imitated treatment methods and high fatality rate, particularly for immunocompromised patients. However, our findings indicated that LNP-H89-Coli@OMV manifested excellent killing stability and superior biosafety, thus implicating a promising clinical candidate.

2. Discussion

To date, the development of antibiotics has significantly fell behind the emergence and widespread dissemination of drug-resistant pathogens, resulting in extremely limited options for effective treatment following pathogen infections. In particular, MDR PAO1 forms the biofilm composed by polysaccharide matrix, fibrin, lipopolysaccharide and other polysaccharide complexes, preventing the penetration of antibiotics, facilitating resistance to stress, and causing the bacteria into a persistent state. Therefore, it is urgent to develop new antibacterial strategies to relieve the increasingly severe crisis of antimicrobial resistance. This pilot study reported for the first time the synergies antibacterial effect of combined H-89 and colistin, which was able to significantly improve the treatment efficacy of MDR infections even for the case that bacteria reached levels above the logarithmic growth phase. Beside the disruption of the bacteria membrane by colistin, it was revealed that H-89 showed the capability to induce apoptosis like bacteria death by comprehensively exanimating the apoptosis hallmakers [43,47,48], including DNA fragmentation, chromosome condensation, caspase increase, membrane depolarization, phosphatidylserine exposure and cell filamentation. Further proteomics and molecular cloning analyses indicate that the bactericidal activity of H89 is associated with the MiaA protein, rather than RecA, ClpX, or ClpP proteins. These findings may further deepen our understanding of cell death mechanisms, such as apoptosis like bacteria death.

Due to the targeting ability LNP-H89-Coli@OMV into the infection areas, it can totally kill the *E. coli,* colistin resistant *Escherichia coli(p_mcr-1), Vibrio parahaemolyticus,* and MDR bacteria in the ESKAPE group including *Klebsiella pneumoniae, Acinetobacter baumannii, Pseudomonas aeruginosa,* and *Enterobacter species*. Besides, LNP-H89-Coli@OMV exhibited the ability to totally eradicate persistent *PAO1* in biofilm. Further *in vivo* biocompatibility experiments demonstrated the physiological safety of LNP-H89-Coli@OMV. Importantly, *in vivo* tests results showed that LNP-H89-Coli@OMV can rapidly accumulated to biofilm PAO1 *in vivo*, significantly eliminating bacterial load in intravenous catheter. Due to their significant antibacterial ability, the immunity response caused by bacteria infection were significantly reduced. Overall, our study has made significant strides in addressing the limitations of antibacterial drugs against persistent PAO1 bacteria. The synergistic compounds H-89 and colistin exhibited promising antibacterial outcomes *in vitro*. Furthermore, by coating engineering OMV, the bacterial-specific biomimetic nanodrugs strongly kill PAO1-infected biofilm (Fig. 4f) and rapidly promoted the targeting ability (Fig. 5d). Therefore, the developed genetically engineered biomimetic liposomal colistin drugs demonstrated the great potential to be translated into clinical applications for treatment of various PAO1-induced diseases, particularly persistent pathogens inside biofilm in the future.

3. Methods

3.1. Bacterial strains and growth conditions

The bacterial strains and plasmids used in this study are listed in Table 1. LB broth, [Miller (Luria–Bertani) (BD, 244620)] was used for all the experiments.

3.2. Plasmid and bacterial strain construction

In this study, the plasmids were constructed by In-Fusion cloning (TaKaRa, 638943). pBAD was linearized by the restriction enzymes NcoI as well as and PstI. pDS132 was linearized by the restriction enzymes XbaI. In-frame deletion mutant was constructed based on SacB-mediated allelic exchange with suicide plasmid pDS132 as described previously [49]. *E. coli* MG1655 was used as the parental strain. The recA, clpX, and clpP deletion and pBAD_clyA-antiPAO1-flag were constructed using the primers from in Table 2.

3.3. Bacterial OMV-antiPAO1-flag and extracellular vesicle preparation

OMV-antiPAO1-flag were prepared in Δ*msbB* (pBAD_*clyA*-antiPAO1-flag) strain following the OMV preparation protocol described previously [35]. Briefly, colonies of bacteria from the LB Agar were picked up and then put in the 20 mL LB, 37 °C, 220 rpm overnight. Then, they were diluted by ratio of 1:100 into fresh LB (BD, 244620), following by being cultured until optical density (OD600) between 0.5 and 0.55 (i.e., exponential phase). 0.1 % arabinose (diluted 1:200 in LB broth) was added to induce the expression of ClyA-antiPAO1-flag protein. After being incubated overnight at 37 °C with shaking (220 rpm), the bacteria were centrifuged at 8000g for 10 min. The supernatant was passed through a 0.45 μm polyvinylidene fluoride filter (Millipore, R8SA47939, USA) and concentrated to 2 mL using 100 kDa ultrafiltration membranes (Millipore, R3EA06699, USA). The concentrate was filtered with a 0.22 μm filter to mitigate any contamination then stored at −20 °C until use. The total protein concentration was quantified using the nanodrop (Thermo Scientific, USA) and bicinchoninic acid protein assay.

3.4. Preparation of LNP-H89-Coli@OMV nanoparticles

The LNP-H89-Coli@OMV nanoparticles were synthesized according to a previous method [50,51], with some modification. H-89 (DC chemical, DC7835), DPPC (Avanti Polar Lipids Inc.), DMPG (Avanti Polar Lipids Inc.) and cholesterol (Avanti Polar Lipids Inc.) were mixed in chloroform, and then the chloroform was evaporated. Then, rotary evaporation was used to make a thin lipid film, which was hydrated in PBS of colistin (sigma, C4461). The hydrated solution was then subjected to freeze–thaw cycles (−196 to 50 °C) to encapsulate colistin and H-89. The dispersions were extruded through polycarbonate membranes to form unilamellar vesicles. Nonencapsulated compounds were removed using the Float-A-Lyzer G2 dialysis device at 4 °C. The OMVs-antiPAO1 with LNP-H89-Coli were extruded through a polycarbonate membrane with 100 nm pore size to yield LNP-H89-Coli@OMV. The loading capacity was measured by using UV–vis absorption spectra and the release of colistin and H-89 from liposome was studied through the absorbance in medium conditions.

Table 1
List of strains used in the study.

Strains	Application
E. coli MG1655	Checkerboard assay, killing assay, animal infection, uptake assay, protein expression, plasmid construction
P. aeruginosae PAO1	Killing assay
A. baumannii ATCC 17978	Killing assay
A. baumannii ATCC BAA-1800	Killing assay
E. coli MG1655(p_mcr-1)	Killing assay
K. pneumoniae ATCC BAA-2146	Killing assay
Salmonella Enteritidis ATCC13076	Killing assay
Citrobacter rodentium DBS100	Killing assay
Vibrio parahaemolyticus RIMD 2210633	Killing assay
E. coli DH5α λ pir	Plasmid construction, Mutant construction
E. coli MDF λ pir	Mutant construction

Table 2
Primer's sequence.

Primer Name	Sequence (5′-3′)
ClyA_PAO1.FOR	atgacgacaagctgcagggtggtggtggtagtggtggt
ClyA_PAO1.REV	cttgtcgtcatcgtctttgtagtctttaatttcaactttggtaccctg
Ide.FOR	acactttgctatgccatagc
Ide.REV	cggcgtttcacttctgagtt
recAFragment 1.FOR	aaggatcgatcctctagtcgttgtgtttaccacccgc
recAFragment 1.REV	tattacccggcatgacaggagtaaaacgacccttgtgtat
recAFragment 2.FOR	cgtcttgtttgatacacaagggtcgttttactcctgtcat
recAFragment 2.REV	gcatgcggtacctctaggccgccgcaggtttaacgccac
clpXFragment 1.FOR	aaaggatcgatcctctagaaagcctctttcggtgttagcg
clpXFragment 1.REV	aatggttaagggtcaaaacctcttctttgttctttgt
clpXFragment 2.FOR	ttttgacccttaaccattcccatacaattagttaaccaaaaagggg
clpXFragment 2.REV	cgcatgcggtacctctagtgaatagctttcatttgctcgttcagatagtactcac
clpPFragment 1.FOR	ggatcgatcctctaggaccttcccggaagaataccac
clpPFragment 1.REV	ctctggcattccgtctcctggataaaattgaaaaaacct
clpPFragment 2.FOR	gacggaatgccagaggcgcaac
clpPFragment 2.REV	atgcggtacctctagaaatcactttatccagaccggcaaac
miaAF1.FOR	aaggatcgatcctctagtccattccggaaaaccgcg
miaAF1.REV	aattgtacacattcaactgatatcactcatctttcaggg
miaAF2.FOR	tgatatcagttgaatgtgtacaattgagacgtatcg
miaAF2.REV	gcatgcggtacctctagtaaaataaggccggtgcggt

3.5. Characterization of the LNP-H89-Coli@OMV nanoparticles

Absorption spectra were obtained by a UV-3101 spectrophotometer. Transmission electron microscope (TEM) images were obtained by using a Tecnai G2 F20 S-Twin at an acceleration voltage of 200 kV. *In vivo* bioimaging analysis was performed using the IVIS Lumina XR system. Confocal laser scanning microscopy (CLSM) images were captured using a Nikon A1R confocal system.

3.6. Animal infection model

Briefly, female mice were used to minimize variations in gender differences. Mice underwent surgery involving subcutaneous implantation of a 1 cm intravenous catheter into their backs, which was loaded with 10^7 CFU of persistent PAO1 bacteria. Twenty-four hours post-surgery, mice were randomly assigned into five groups (n = 6 each). Treatment administration began with repeated lateral tail vein injections according to the following regimens: (1) Control (2 mg/kg), (2) LNP-H89 (2 mg/kg, contain H-89 ~ 20 μg/kg), (3) LNP-Coli (2 mg/kg, contain coli ~2 μg/kg), (4) LNP-H89-Coli (2 mg/kg, contain H-89 ~ 20 μg/kg and coli ~2 μg/kg), and (5) LNP-H89-Coli@OMV (2 mg/kg, contain H-89 ~ 13.33 μg/kg and coli ~1.33 μg/kg). Treatments were administered every 12 h over a period of three days. At 24 h following the final treatment, mice were humanely euthanized, and the intact catheters were retrieved and sonicated in 1 mL of sterile 1× PBS. The resulting homogenates were subjected to a 10-fold serial dilution, with 100 μL aliquots of each dilution plated onto LB agar for the enumeration of surviving bacteria. Furthermore, the whole infected skin areas were meticulously excised and processed for paraffin embedding to prepare them for histological sectioning. Subsequently, Hematoxylin and Eosin (H&E) staining was performed on these sections for histopathological evaluation. All animal experiments were conducted in compliance with and approved by the Panel on Research Ethics at the University of Macau

and Guangxi University (Ethics Approval Number: UMARE-033-2020 and GXU-2024-202).

CRediT authorship contribution statement

Xianyuan Wei: Writing – review & editing, Writing – original draft, Visualization, Software, Resources, Methodology, Investigation, Formal analysis, Conceptualization. **Jintong Guo:** Visualization, Software, Resources, Investigation. **Xiaorui Geng:** Visualization, Validation, Resources, Investigation. **Yuhao Chen:** Visualization, Validation, Investigation. **Xianfang Wei:** Software, Resources, Investigation. **Bin Liu:** Visualization, Investigation. **Jun Zheng:** Supervision, Methodology, Conceptualization. **Zhen Yuan:** Writing – review & editing, Supervision, Resources, Project administration, Methodology, Funding acquisition, Formal analysis, Data curation, Conceptualization.

Declaration of competing interest

The authors declare that they have no known competing financial interests or personal relationships that could have appeared to influence the work reported in this paper.

Data availability

I have shared my data in supporting information.

Acknowledgements

We thank professor Songnan Qu, the Animal Research Core, Biological Imaging and Stem Cell Core, Guangxi University and University of Macau for assistance on this project.

This work was also supported by the University of Macau (MYRG2020-00067-FHS, MYRG-GRG2023-00038-FHS and MYRG2022-00054-FHS), Macao Science and Technology Development Fund (FDCT 0020/2019/AMJ and FDCT 0048/2021/AGJ), and Natural Science Foundation of Guangdong Province (EF017/FHS-YZ/2021/GDST).

Appendix A. Supplementary data

Supplementary data to this article can be found online at https://doi.org/10.1016/j.cej.2024.154515.

References

[1] C. Antimicrobial Resistance, Global burden of bacterial antimicrobial resistance in 2019: a systematic analysis, Lancet 399 (10325) (2022) 629–655, https://doi.org/10.1016/S0140-6736(21)02724-0.

[2] R.F. Seipke, Antibiotics made to order, Science 376 (6596) (2022) 919–920, https://doi.org/10.1126/science.abq3206.

[3] J.S. Guðmundsdóttir, E.G.A. Fredheim, C.I.M. Koumans, J. Hegstad, P.C. Tang, D. I. Andersson, Ø. Samuelsen, P.J. Johnsen, The chemotherapeutic drug methotrexate selects for antibiotic resistance, EBioMedicine 74 (2021) 103742, https://doi.org/10.1016/j.ebiom.2021.103742.

[4] I. Levin-Reisman, I. Ronin, O. Gefen, I. Braniss, N. Shoresh, N.Q. Balaban, Antibiotic tolerance facilitates the evolution of resistance, Science 355 (6327) (2017) 826–830, https://doi.org/10.1126/science.aaj2191.

[5] Y.X. Ma, C.Y. Wang, Y.Y. Li, J. Li, Q.Q. Wan, J.H. Chen, F.R. Tay, L.N. Niu, Considerations and caveats in combating ESKAPE pathogens against nosocomial infections, Adv. Sci. (Weinh.) 7 (1) (2020) 1901872, https://doi.org/10.1002/advs.201901872.

[6] M. Baym, L.K. Stone, R. Kishony, Multidrug evolutionary strategies to reverse antibiotic resistance, Science 351 (6268) (2016) aad3292, https://doi.org/10.1126/science.aad3292.

[7] V. Lazar, O. Snitser, D. Barkan, R. Kishony, Antibiotic combinations reduce Staphylococcus aureus clearance, Nature 610 (7932) (2022) 540–546, https://doi.org/10.1038/s41586-022-05260-5.

[8] M. Stracy, O. Snitser, I. Yelin, Y. Amer, M. Parizade, R. Katz, G. Rimler, T. Wolf, E. Herzel, G. Koren, J. Kuint, B. Foxman, G. Chodick, V. Shalev, R. Kishony, Minimizing treatment-induced emergence of antibiotic resistance in bacterial infections, Science 375 (6583) (2022) 889–894, https://doi.org/10.1126/science.abg9868.

[9] Y.Y. Liu, Y. Wang, T.R. Walsh, L.X. Yi, R. Zhang, J. Spencer, Y. Doi, G. Tian, B. Dong, X. Huang, L.F. Yu, D. Gu, H. Ren, X. Chen, L. Lv, D. He, H. Zhou, Z. Liang, J.H. Liu, J. Shen, Emergence of plasmid-mediated colistin resistance mechanism MCR-1 in animals and human beings in China: a microbiological and molecular biological study, Lancet Infect. Dis. 16 (2) (2016) 161–168, https://doi.org/10.1016/S1473-3099(15)00424-7.

[10] M. Song, Y. Liu, T. Li, X. Liu, Z. Hao, S. Ding, P. Panichayupakaranant, K. Zhu, J. Shen, Plant natural flavonoids against multidrug resistant pathogens, Adv. Sci. (Weinh.) 8 (15) (2021) e2100749, https://doi.org/10.1002/advs.202100749.

[11] C. Pearman, W. Kent, N. Bracken, M. Hussain, H-89 inhibits transient outward and inward rectifier potassium currents in isolated rat ventricular myocytes, Br. J. Pharmacol. 148 (8) (2006) 1091–1098, https://doi.org/10.1038/sj.bjp.0706810.

[12] Y. Jiang, V.T. Puliyappadamba, L. Zhang, W. Wu, A. Wali, M.B. Yaffe, J.A. Fontana, A.K. Rishi, A novel mechanism of cell growth regulation by Cell Cycle and Apoptosis Regulatory Protein (CARP)-1, J. Mol. Signal 5 (2010) 7, https://doi.org/10.1186/1750-2187-5-7.

[13] C.C. Augusto Pessina, N. Savalli, A. Bonomi, L. Cavicchini, E. Turlizzi, F. Guizzardi, L. Guido, L. Daprai, M.G. Neri, Bcl-2 down modulation in WEHI-3B/CTRES cells resistant to Cholera Toxin (CT)-induced apoptosis, Cell Res. 16 (3) (2006) 306–312.

[14] K.W. Karissa, J. Muñoz, Lauren M. Sheehan, Ming Tan, Christine Sütterlin, The small molecule H89 inhibits chlamydia inclusion growth and production of infectious progeny, Infect. Immun. 89 (7) (2021) e0072920.

[15] K. Dib, A. El Banna, C. Radulescu, G.L. Campos, G. Sheehan, K. Kavanagh, Histamine produced by gram-negative bacteria impairs neutrophil's antimicrobial response by engaging the histamine 2 receptor, J. Innate Immun. (2022) 1–21, https://doi.org/10.1159/000525536.

[16] C. Kuijl, N.D. Savage, M. Marsman, A.W. Tuin, L. Janssen, D.A. Egan, M. Ketema, R. van den Nieuwendijk, S.J. van den Eeden, A. Geluk, A. Poot, G. van der Marel, R. L. Beijersbergen, H. Overkleeft, T.H. Ottenhoff, J. Neefjes, Intracellular bacterial growth is controlled by a kinase network around PKB/AKT1, Nature 450 (7170) (2007) 725–730.

[17] S.K. Forslund, R. Chakaroun, M. Zimmermann-Kogadeeva, L. Marko, J. Aron-Wisnewsky, T. Nielsen, L. Moitinho-Silva, T.S.B. Schmidt, G. Falony, S. Vieira-Silva, S. Adriouch, R.J. Alves, K. Assmann, J.P. Bastard, T. Birkner, R. Caesar, J. Chilloux, L.P. Coelho, L. Fezeu, N. Galleron, G. Helft, R. Isnard, B. Ji, M. Kuhn, E. Le Chatelier, A. Myridakis, L. Olsson, N. Pons, E. Prifti, B. Quinquis, H. Roume, J. E. Salem, N. Sokolovska, V. Tremaroli, M. Valles-Colomer, C. Lewinter, N. B. Sondertoft, H.K. Pedersen, T.H. Hansen, C. MetaCardis, J.P. Gotze, L. Kober, H. Vestergaard, T. Hansen, J.D. Zucker, S. Hercberg, J.M. Oppert, I. Letunic, J. Nielsen, F. Backhed, S.D. Ehrlich, M.E. Dumas, J. Raes, O. Pedersen, K. Clement, M. Stumvoll, P. Bork, Combinatorial, additive and dose-dependent drug-microbiome associations, Nature 600 (7889) (2021) 500–505, https://doi.org/10.1038/s41586-021-04177-9.

[18] K. Andries, P. Verhasselt, J. Guillemont, H.W. Gohlmann, J.M. Neefs, H. Winkler, J. Van Gestel, P. Timmerman, M. Zhu, E. Lee, P. Williams, D. de Chaffoy, E. Huitric, S. Hoffner, E. Cambau, C. Truffot-Pernot, N. Lounis, V. Jarlier, A diarylquinoline drug active on the ATP synthase of Mycobacterium tuberculosis, Science 307 (5707) (2005) 223–227, https://doi.org/10.1126/science.1106753.

[19] A.R. Brochado, A. Telzerow, J. Bobonis, M. Banzhaf, A. Mateus, J. Selkrig, E. Huth, S. Bassler, J. Zamarreno Beas, M. Zietek, N. Ng, S. Foerster, B. Ezraty, B. Py, F. Barras, M.M. Savitski, P. Bork, S. Gottig, A. Typas, Species-specific activity of antibacterial drug combinations, Nature 559 (7713) (2018) 259–263, https://doi.org/10.1038/s41586-018-0278-9.

[20] M. Ye, Y. Zhao, Y. Wang, M. Zhao, N. Yodsanit, R. Xie, D. Andes, S. Gong, A dual-responsive antibiotic-loaded nanoparticle specifically binds pathogens and overcomes antimicrobial-resistant infections, Adv. Mater. 33 (9) (2021) e2006772, https://doi.org/10.1002/adma.202006772.

[21] S. Gao, X. Yan, G. Xie, M. Zhu, X. Ju, P.J. Stang, Y. Tian, Z. Niu, Membrane intercalation-enhanced photodynamic inactivation of bacteria by a metallacycle and TAT-decorated virus coat protein, PNAS 116 (47) (2019) 23437–23443, https://doi.org/10.1073/pnas.1911869116.

[22] S. Hussain, J. Joo, J. Kang, B. Kim, G.B. Braun, Z.G. She, D. Kim, A.P. Mann, T. Molder, T. Teesalu, S. Carnazza, S. Guglielmino, M.J. Sailor, E. Ruoslahti, Antibiotic-loaded nanoparticles targeted to the site of infection enhance antibacterial efficacy, Nat. Biomed. Eng. 2 (2) (2018) 95–103, https://doi.org/10.1038/s41551-017-0187-5.

[23] R.H. Fang, W. Gao, L. Zhang, Targeting drugs to tumours using cell membrane-coated nanoparticles, Nat. Rev. Clin. Oncol. 20 (1) (2023) 33–48, https://doi.org/10.1038/s41571-022-00699-x.

[24] A. Cubillos-Ruiz, M.A. Alcantar, N.M. Donghia, P. Cardenas, J. Avila-Pacheco, J. J. Collins, An engineered live biotherapeutic for the prevention of antibiotic-induced dysbiosis, Nat. Biomed. Eng. 6 (7) (2022) 910–921, https://doi.org/10.1038/s41551-022-00871-9.

[25] W. Huang, C. Shu, L. Hua, Y. Zhao, H. Xie, J. Qi, F. Gao, R. Gao, Y. Chen, Q. Zhang, W. Li, M. Yuan, C. Ye, Y. Ma, Modified bacterial outer membrane vesicles induce autoantibodies for tumor therapy, Acta Biomater. 108 (2020) 300–312, https://doi.org/10.1016/j.actbio.2020.03.030.

[26] C. Schwechheimer, M.J. Kuehn, Outer-membrane vesicles from Gram-negative bacteria: biogenesis and functions, Nat. Rev. Microbiol. 13 (10) (2015) 605–619, https://doi.org/10.1038/nrmicro3525.

[27] Y. Wu, G. Deng, Z. Song, K. Zhang, J. Deng, K. Jiang, H. Han, Enhancing antibacterial immunotherapy for bacterial pneumonia via nanovaccines coated with outer membrane vesicles, Chem. Eng. J. 436 (2022) 135040, https://doi.org/10.1016/j.cej.2022.135040.

[28] R. Langer, Drug delivery and targeting, Nature 392 (6679 Suppl) (1998) 5–10.

[29] S.M. Lehar, T. Pillow, M. Xu, L. Staben, K.K. Kajihara, R. Vandlen, L. DePalatis, H. Raab, W.L. Hazenbos, J.H. Morisaki, J. Kim, S. Park, M. Darwish, B.C. Lee, H. Hernandez, K.M. Loyet, P. Lupardus, R. Fong, D. Yan, C. Chalouni, E. Luis, Y. Khalfin, E. Plise, J. Cheong, J.P. Lyssikatos, M. Strandh, K. Koefoed, P. S. Andersen, J.A. Flygare, M. Wah Tan, E.J. Brown, S. Mariathasan, Novel antibody-antibiotic conjugate eliminates intracellular S. aureus, Nature 527 (7578) (2015) 323–328, https://doi.org/10.1038/nature16057.

[30] Y. Imamura, K. Yanagihara, Y. Fukuda, Y. Kaneko, M. Seki, K. Izumikawa, Y. Miyazaki, Y. Hirakata, T. Sawa, J.P. Wiener-Kronish, Effect of anti-PcrV antibody in a murine chronic airway Pseudomonas aeruginosa infection model, Eur. Respir. J. 29 (5) (2007) 965.

[31] A. DiGiandomenico, A.E. Keller, C. Gao, G.J. Rainey, P. Warrener, M.M. Camara, J. Bonnell, R. Fleming, B. Bezabeh, N. Dimasi, B.R. Sellman, J. Hilliard, C. M. Guenther, V. Datta, W. Zhao, C. Gao, X.Q. Yu, J.A. Suzich, C.K. Stover, A multifunctional bispecific antibody protects against Pseudomonas aeruginosa, Sci. Transl. Med. 6 (262) (2014) 262ra155, https://doi.org/10.1126/scitranslmed.3009655.

[32] C.K. Alexander Simonis, Alexandra Albus, Katharina Rox, Biao Yuan, Dmitriy Holzmann, Joana A Wilms, Sylvia Zuber, Lisa Kottege, Sandra Winter, Meike Meyer, Kristin Schmitt, Henning Gruell, Sebastian J Theobald, Anna-Maria Hellmann, Christina Meyer, Meryem Seda Ercanoglu, Nina Cramer, Antje Munder, Michael Hallek, Gerd Fätkenheuer, Manuel Koch, Harald Seifert, Ernst Rietschel, Thomas C Marlovits, Silke van Koningsbruggen-Rietschel, Florian Klein, Jan Rybniker, Discovery of highly neutralizing human antibodies targeting Pseudomonas aeruginosa, Cell S0092-8674(23)01084-X (2023). https://doi.org/10.1016/j.cell.2023.10.002.

[33] Y. Yue, J. Xu, Y. Li, K. Cheng, Q. Feng, X. Ma, N. Ma, T. Zhang, X. Wang, X. Zhao, G. Nie, Antigen-bearing outer membrane vesicles as tumour vaccines produced in situ by ingested genetically engineered bacteria, Nat. Biomed. Eng. 6 (7) (2022) 898–909, https://doi.org/10.1038/s41551-022-00886-2.

[34] R.H. Fang, A.V. Kroll, W. Gao, L. Zhang, Cell membrane coating nanotechnology, Adv. Mater. 30 (23) (2018) e1706759, https://doi.org/10.1002/adma.201706759.

[35] Y. Li, R. Zhao, K. Cheng, K. Zhang, Y. Wang, Y. Zhang, Y. Li, G. Liu, J. Xu, J. Xu, G. J. Anderson, J. Shi, L. Ren, X. Zhao, G. Nie, Bacterial outer membrane vesicles presenting programmed death 1 for improved cancer immunotherapy via immune activation and checkpoint inhibition, ACS Nano 14 (12) (2020) 16698–16711, https://doi.org/10.1021/acsnano.0c03776.

[36] T. Manso, A. Kushwaha, N. Abdollahi, P. Duroux, V. Giudicelli, S. Kossida, Mechanisms of action of monoclonal antibodies in oncology integrated in IMGT/mAb-DB, Front. Immunol. 14 (2023) 1129323, https://doi.org/10.3389/fimmu.2023.1129323.

[37] J.F. Toso, V.J. Gill, P. Hwu, F.M. Marincola, N.P. Restifo, D.J. Schwartzentruber, R. M. Sherry, S.L. Topalian, J.C. Yang, F. Stock, L.J. Freezer, K.E. Morton, C. Seipp, L. Haworth, S. Mavroukakis, D. White, S. MacDonald, J. Mao, M. Sznol, S. A. Rosenberg, Phase I study of the intravenous administration of attenuated Salmonella typhimurium to patients with metastatic melanoma, J. Clin. Oncol. 20 (1) (2002) 142–152, https://doi.org/10.1200/JCO.2002.20.1.142.

[38] X. Wei, M. Du, Z. Chen, Z. Yuan, Recent advances in bacteria-based cancer treatment, Cancers (basel) 14 (19) (2022), https://doi.org/10.3390/cancers14194945.

[39] G. Orhan, A. Bayram, Y. Zer, I. Balci, Synergy tests by E test and checkerboard methods of antimicrobial combinations against Brucella melitensis, J. Clin. Microbiol. 43 (1) (2005) 140–143, https://doi.org/10.1128/JCM.43.1.140-143.2005.

[40] J. Li, R.L. Nation, J.D. Turnidge, R.W. Milne, K. Coulthard, C.R. Rayner, D. L. Paterson, Colistin: the re-emerging antibiotic for multidrug-resistant Gram-negative bacterial infections, Lancet Infect. Dis. 6 (9) (2006) 589–601, https://doi.org/10.1016/S1473-3099(06)70580-1.

[41] A.G. Thea Brennan-Krohn, S. Rodriguez, J.E. Kirby, A.M. Earl, Transcriptomics reveals how minocycline-colistin synergy overcomes antibiotic resistance in multidrug-resistant klebsiella pneumoniae, Antimicrob. Agents Chemother. 66 (3) (2022) e0196921.

[42] Y.W. Jingchun Kong, Zhuocheng Yao, Yishuai Lin, Yi Zhang, Yijia Han, Tieli Zhou, Jianzhong Ye, Jianming Cao, Eugenol works synergistically with colistin against colistin-resistant Pseudomonas aeruginosa and Klebsiella pneumoniae isolates by enhancing membrane permeability, Microbiol. Spectrum 11(5) (2023) e0366622.

[43] D.J. Dwyer, D.M. Camacho, M.A. Kohanski, J.M. Callura, J.J. Collins, Antibiotic-induced bacterial cell death exhibits physiological and biochemical hallmarks of apoptosis, Mol. Cell 46 (5) (2012) 561–572, https://doi.org/10.1016/j.molcel.2012.04.027.

[44] O. Méhi, B. Bogos, B. Csörgo, C. Pál, Genomewide screen for modulators of evolvability under toxic antibiotic exposure, Antimicrob. Agents Chemother. 57 (7) (2013) 3453–3456, https://doi.org/10.1128/aac.02454-12.

[45] T.G. Hagervall, J.U. Ericson, K.B. Esberg, J.N. Li, G.R. Björk, Role of tRNA modification in translational fidelity, Biochim. Biophys. Acta 1050 (1–3) (1990) 263–266, https://doi.org/10.1016/0167-4781(90)90178-5.

[46] P. Gollnick, C. Yanofsky, tRNA(Trp) translation of leader peptide codon 12 and other factors that regulate expression of the tryptophanase operon, J. Bacteriol. 172 (6) (1990) 3100–3107, https://doi.org/10.1128/jb.172.6.3100-3107.1990.

[47] F. Wong, J.M. Stokes, S.C. Bening, C. Vidoudez, S.A. Trauger, J.J. Collins, Reactive metabolic byproducts contribute to antibiotic lethality under anaerobic conditions, Mol. Cell 82(18) (2022) 3499-3512 e10. https://doi.org/10.1016/j.molcel.2022.07.009.

[48] E. Liu, Y. Chen, J. Xu, S. Gu, N. An, J. Xin, W. Wang, Z. Liu, Q. An, J. Yi, W. Yin, Platelets inhibit methicillin-resistant staphylococcus aureus by inducing hydroxyl radical-mediated apoptosis-like cell death, Microbiol. Spectr. 10 (4) (2022) e0244121, https://doi.org/10.1128/spectrum.02441-21.

[49] J. Zheng, S.L. Tung, K.Y. Leung, Regulation of a type III and a putative secretion system in Edwardsiella tarda by EsrC is under the control of a two-component system, EsrA-EsrB, Infect. Immun. 73 (7) (2005) 4127–4137, https://doi.org/10.1128/IAI.73.7.4127-4137.2005.

[50] H. Xu, T.Y. Ohulchanskyy, A. Yakovliev, R. Zinyuk, J. Song, L. Liu, J. Qu, Z. Yuan, Nanoliposomes co-encapsulating CT imaging contrast agent and photosensitizer for enhanced, imaging guided photodynamic therapy of cancer, Theranostics 9 (5) (2019) 1323–1335, https://doi.org/10.7150/thno.31079.

[51] Z. Wang, Y. Ma, H. Khalil, R. Wang, T. Lu, W. Zhao, Y. Zhang, J. Chen, T. Chen, Fusion between fluid liposomes and intact bacteria: study of driving parameters and *in vitro* bactericidal efficacy, Int. J. Nanomed. 11 (2016) 4025–4036, https://doi.org/10.2147/IJN.S55807.